Supplementary Material

Calcium microdomains at the immunological synapse: how ORAI channels, mitochondria and calcium pumps generate local calcium signals for efficient T-cell activation

Ariel Quintana[1,6,7*], Mathias Pasche[2,6,*], Christian Junker[1*], Dalia Al-Ansary[1], Heiko Rieger[3], Carsten Kummerow[1], Lucia Nuñez[4], Carlos Villalobos[4], Paul Meraner[5], Ute Becherer[2], Jens Rettig[2], Barbara A Niemeyer[1] & Markus Hoth[1,7]

[1]Department of Biophysics, [2]Department of Physiology, University of Saarland, 66421 Homburg, Germany. [3]Department of Theoretical Physics, Saarland University, 66041 Saarbrücken, Germany, [4]Institute of Biology and Molecular Genetics, University of Valladolid and CSIC, 47003 Valladolid, Spain, [5]La Jolla Institute for Allergy & Immunology, La Jolla, CA 92037, USA

*These authors contributed equally to this paper

[6]Current address:
Ariel Quintana: La Jolla Institute for Allergy& Immunology, La Jolla, CA 92037, USA and Department of Pathology, Immune Disease Institute, Harvard University, 200 Longwood Avenue, Room 152 Boston, MA 02115, USA.
Mathias Pasche: MRC Laboratory of Molecular Biology, Hills Road, Cambridge, UK.

[7]Please address correspondence to:
Ariel Quintana and Markus Hoth
Email: quintana@liai.org or quintana@idi.harvard.edu and markus.hoth@uks.eu

Supplementary Figure 1

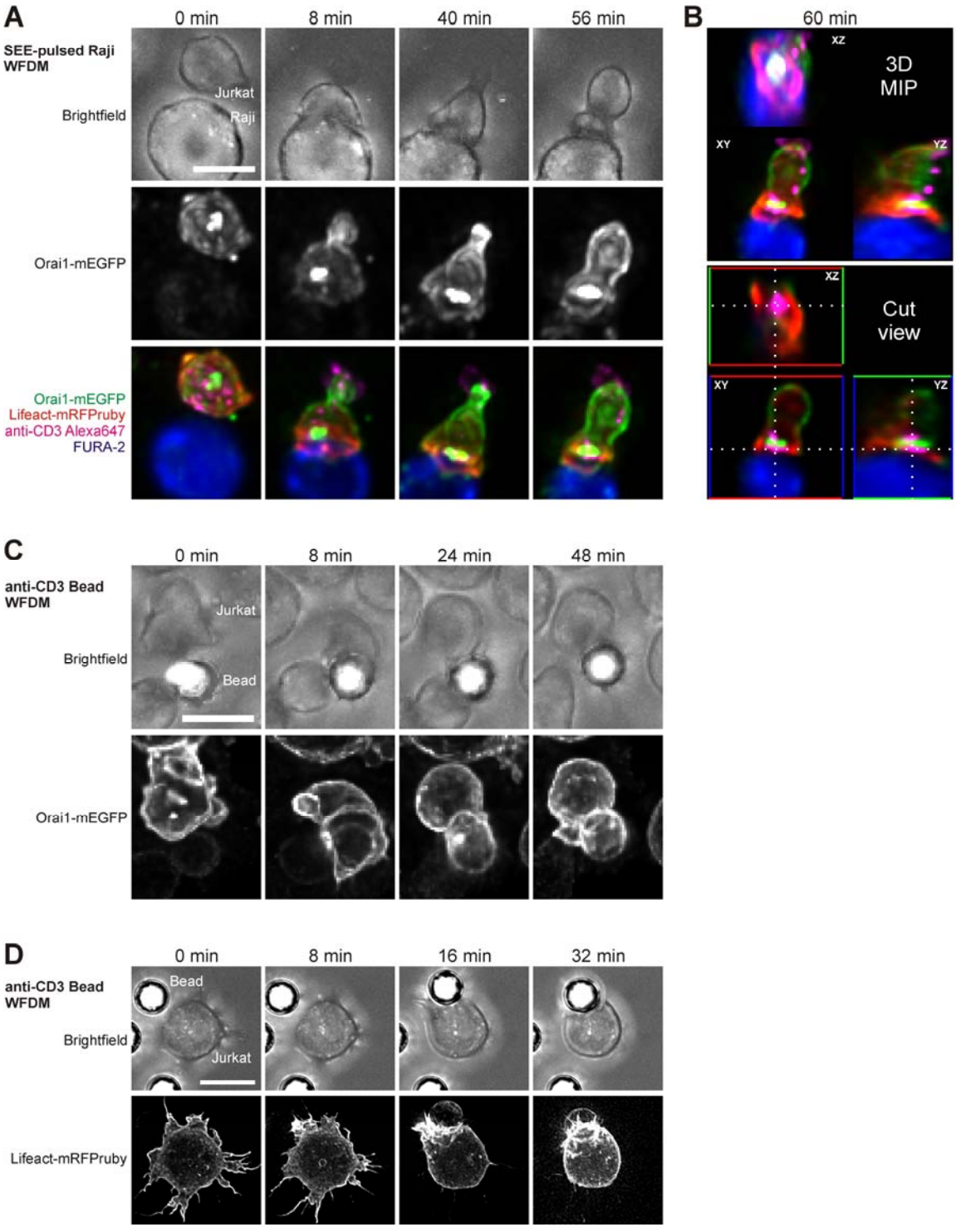

Supplementary Figure 1 ORAI1 localization during IS formation. (**A**) Widefield deconvolution microscopy (WFDM) imaging of a Jurkat T-cell contacting a SEE-pulsed Raji B-cell which was stained with fura-2/AM (blue). The T-cell was transfected with ORAI1-mEGFP and Lifeact-mRFPruby but not with STIM1. Displayed as XY maximum intensity projections (MIP), intracellular ORAI1-mEGFP (green) is quickly translocated towards the IS (bright dot) while plasmalemmal ORAI1-mEGFP first accumulates at the distal pole before being translocated towards the IS. Fast appearance of a ring-shaped actin-pattern (Lifeact-mRFPruby, red) and central accumulation of CD3 (stained with anti-CD3 Alexa647, magenta) at later time points confirm the generation of a stable IS. Statistical analysis, see **Fig. 1B**. (**B**) The fast accumulating, dot-like structure of ORAI1-mEGFP is not located in the plasmamembrane as seen on the MIP and cut-view pictures of the T-cell from panel A 60 min after contact with the Raji B-cell. The cut-view shows the IS in XY, XZ and YZ. ORAI1-mEGFP (green) is located inside the cell relative to the cSMAC-located CD3 accumulation (magenta). (**C**) An ORAI1-mEGFP expressing Jurkat T-cell makes contact with an anti-CD3 antibody-coated 6 µm bead. As seen after contact with the SEE-pulsed Raji cells, ORAI1-mEGFP first concentrates at the distal pole before being slightly enriched at the IS. Statistical analysis, see Figure 1**C**. (**D**) A Lifeact-mRFPruby expressing Jurkat T-cell makes contact with an anti-CD3 antibody-coated 6 µm bead. Scale bars are 10 µm.

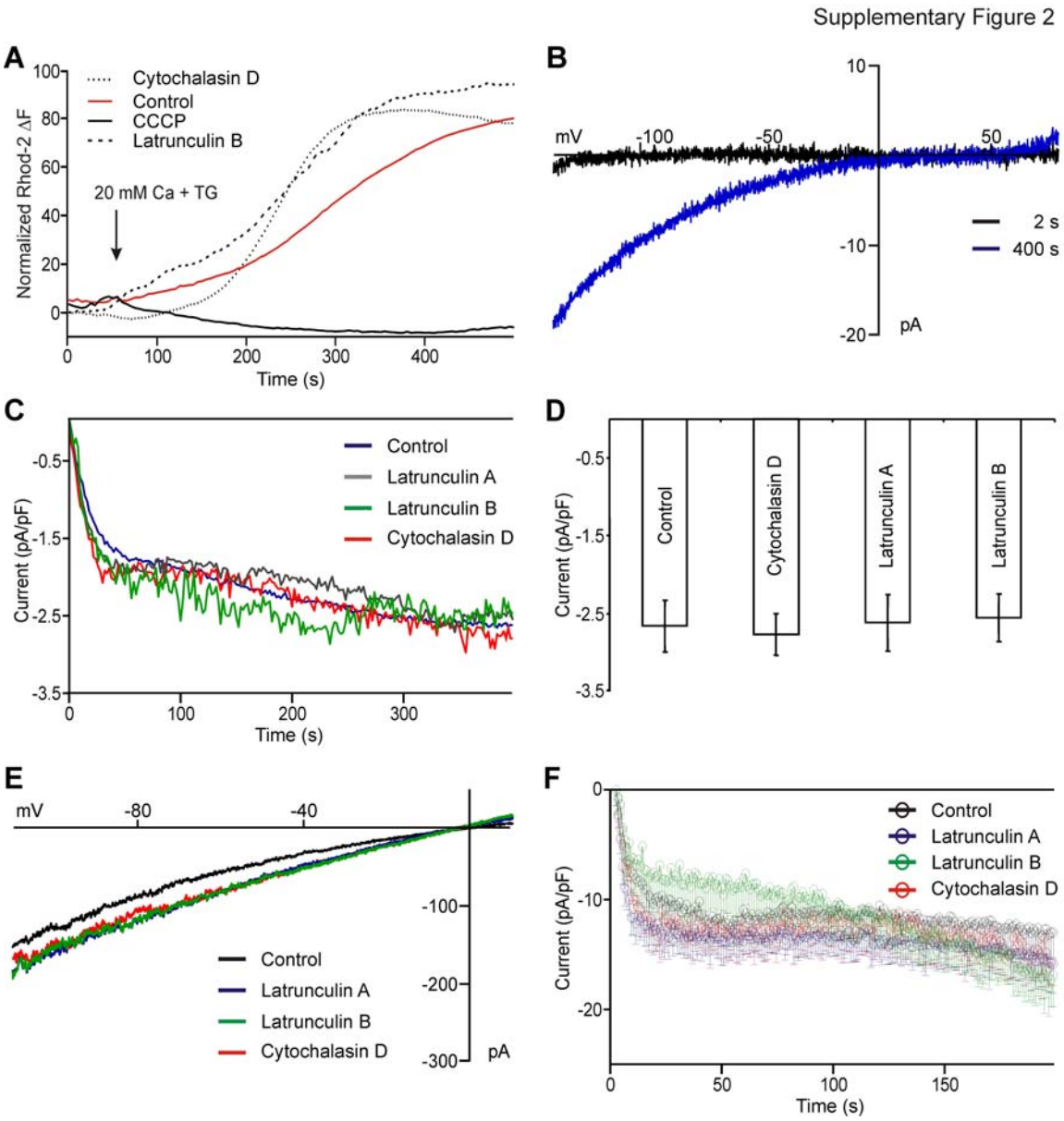

Supplementary Figure 2 Cytoskeleton polymerization disrupting drugs do not inhibit mitochondrial Ca^{2+} uptake, ORAI currents and Ca^{2+}-activated K^+ channel activity. (**A**) Average of normalized rhod-2 fluorescence from Jurkat T-cells in the presence or in the absence of actin cytoskeleton polymerization disrupting drugs following stimulation with 1 μM TG in 20 mM Ca^{2+} containing solution. Note that the drugs do not inhibit the Ca^{2+} entry into mitochondria as CCCP does by disrupting mitochondrial membrane potential

and thereby blocking mitochondrial Ca^{2+} uptake independently of Ca^{2+} microdomain levels close to mitochondrial uniporter. (**B**) Average current-voltage (I/V) relationships of ORAI1 currents from Jurkat T-cells at 2 (black trace) and 400 (blue trace) seconds after establishing the whole-cell configuration. Currents were acquired using a 200 ms voltage ramp spanning from –150 to +100 mV applied at 2 seconds intervals. Note the absence of outward current at positive membrane voltages, which is a prominent feature of the ORAI channel I/V curve. (**C**) Average ORAI1 currents from control cells shown in (**B**) and from cells pre-treated with actin cytoskeleton polymerization disrupting drugs, as indicated. Current sizes are shown at –130 mV, normalized to the cell size, averaged and plotted versus time. Currents were leak-corrected by subtracting averages of the currents from the first three voltage ramps before ORAI channel activation. (**D**) Statistical analysis of ORAI1 currents 350 seconds after establishing the whole cell configuration shows no significant differences between control cells and cells treated with the respective cytoskeleton drugs (control: $n = 14$, cytochalasin D: $n = 7$, Latrunculin A: $n = 8$, Latrunculin B: $n = 8$; $p = 0.89$, $p = 0.78$, $p = 0.88$). (**E**) Average current-voltage (I/V) relationships of Ca^{2+}-activated K^+ currents from Jurkat T-cells in the presence or absence of actin cytoskeleton polymerization disrupting drugs, as indicated, at 200 seconds after establishing the whole-cell configuration. Currents were acquired using a 200 ms voltage ramp spanning from –120 to +20 mV applied at 2 s intervals. (**F**) Average of Ca^{2+}-activated K^+ currents from cells shown in (**E**). Current sizes were measured at –80 mV, normalized to the cell size, averaged and plotted versus time. Currents were leak-corrected by subtracting averages of the currents from the first three voltage ramps before Ca^{2+}-activated K^+ channel activation. Note the absence of significant differences between

control and treated cells (control: $n = 14$, cytochalasin D: $n = 5$, Latrunculin A: $n = 8$, Latrunculin B: $n = 4$; $p = 0.3$, $p = 0.59$, $p = 0.82$).

Supplementary Figure 3

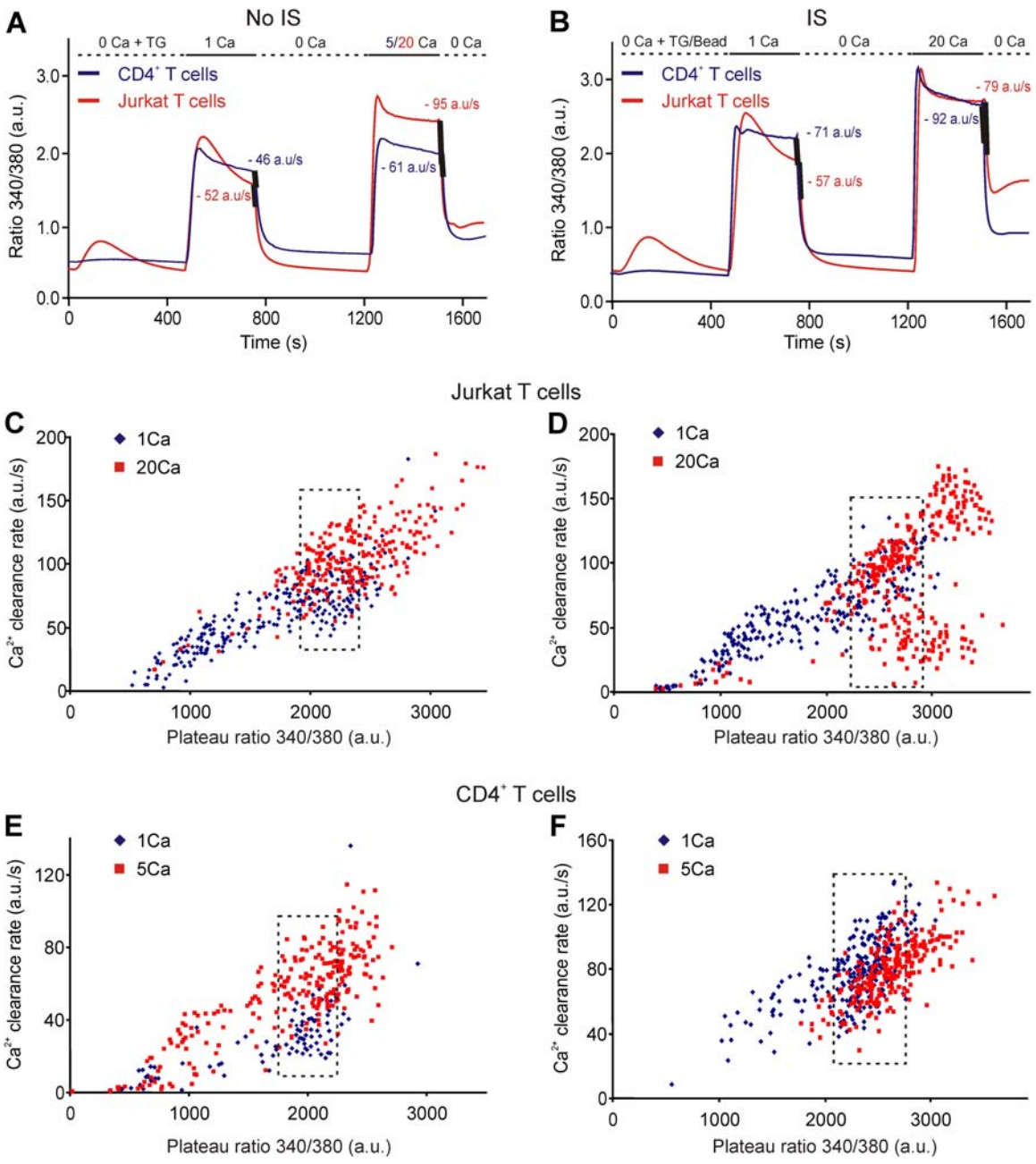

Supplementary Figure 3 PMCA activity in T-cells as a function of global Ca^{2+} signals. (**A**) Average of $[Ca^{2+}]_i$ responses induced by either 1 or 20 mM extracellular Ca^{2+} solutions in Jurkat T cells (red traces) or induced by 1 or 5 mM in $CD4^+$ T-cells (blue traces) following TG stimulation (No IS). The averages of Ca^{2+} clearance rates following $[Ca^{2+}]_i$ elevation, indicated by the thick lines, were calculated from the dRatio (340/380)/d*t* slopes over 10 s periods following $[Ca^{2+}]_o$ removal ($n = 931$, $p < 0.001$, $n = 253$, $p < 0.001$ respectevely). (**B**) Same experiments and analysis as in (**A**) only that T-cells were stimulated with both anti-CD3 antibody-coated beads in order to induce the formation of the IS and TG to ensure maximal activation of ORAI1 channels ($n = 405$, $p < 0.001$, $n = 113$, $p < 0.001$ respectively). (**C** and **D**) Ca^{2+} clearance rate as a function of ratio (340/380) from Jurkat single T-cells following exposure to different $[Ca^{2+}]_o$. One representative plot from one out of four experiments as the ones shown in **A** and **B**. Each symbol represents the initial rate of Ca^{2+} clearance after removal of the extracellular Ca^{2+} containing solution plotted against the preceding $[Ca^{2+}]_i$ plateaus, which were taken from the exposure to 1 mM (◊ blue) or 20 mM (□ red) extracellular Ca^{2+} solution. The dashed black rectangle highlights those cells (30 %) in which 1 and 20 mM $[Ca^{2+}]_o$ evoked the same global ratio (340/380) plateaus (iso-cells) but different cytosolic Ca^{2+} clearance rates. Notice that PMCA activity is enhanced (called modulation) with the increase of the extracellular Ca^{2+} concentration (from 1 to 20 mM) in iso-cells following No IS (**C**) stimulation but not after IS (**D**) stimualtion. (**E** and **F**) Same analysis as in (**C**, **D**) but for $CD4^+$ T-cells. Results regarding PMCA modulation were the same. Traces and Ca^{2+} clerance rate from Jurkat and $CD4^+$ iso-cells are shown in Fig. **6A** and **B,** respectively.

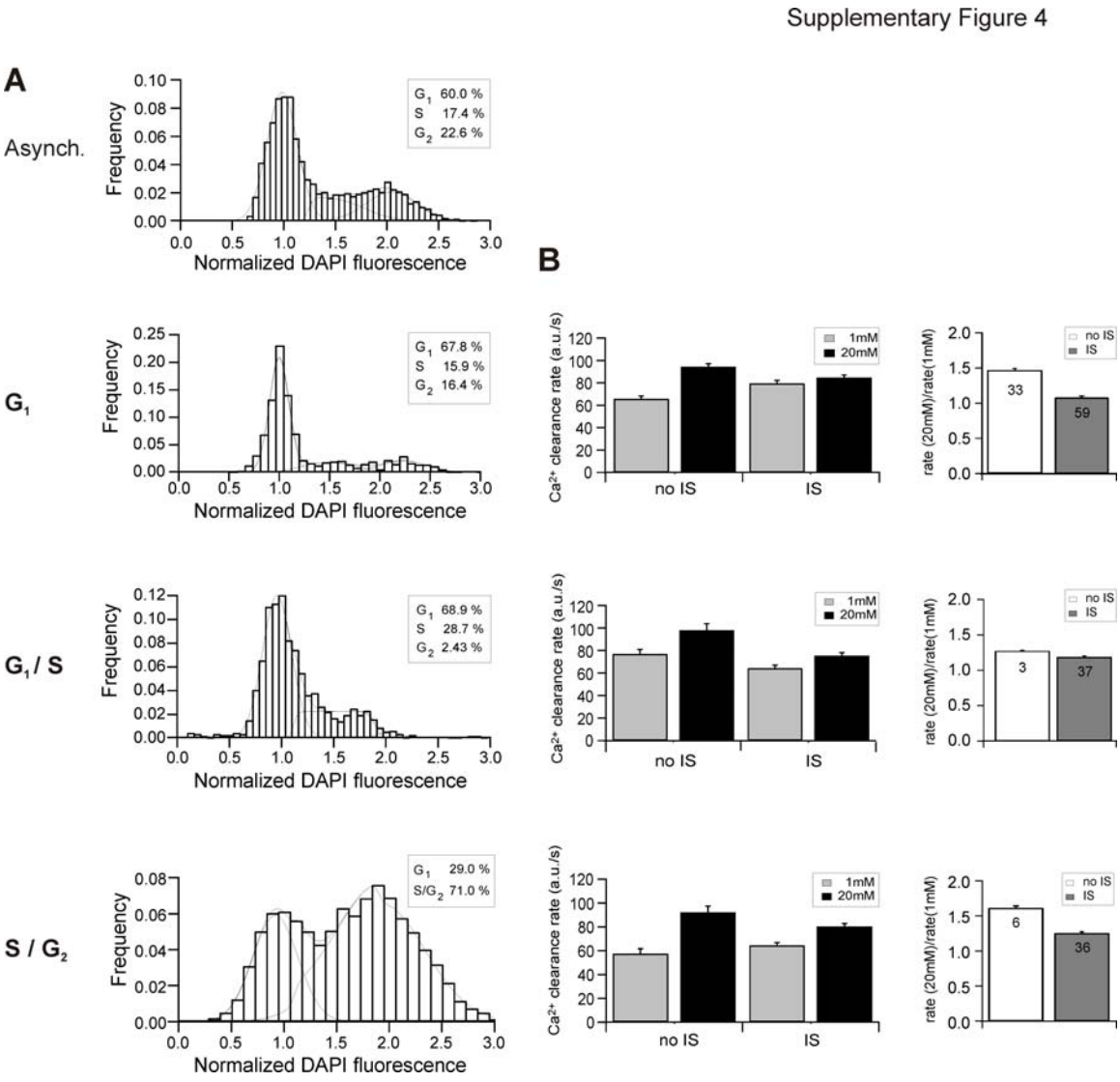

Supplementary Figure 4 Modulation of PMCA activity by Ca^{2+} microdomains during the cell cycle. (**A**) DNA content of Jurkat T cells in different phases of the cell cycle as measured by the intensity of their DAPI fluorescence. Cells were arrested in G_1 and G_1/S transition and then released to S phase. Unsynchronized cells are shown as control. Histograms of single cell DAPI fluorescence (densitometric sum) were fitted to quantify the proportion of cells in each cycle phase. For the last condition there was no

dependence on the S phase parameters of the fit equation, so the proportion of cells is shown as S/G_2 combined. Histograms were normalized to the peak category within the G_1 distribution. For each condition at least 660 cells were analyzed. (**B**) Ca^{2+} clearance rates of Jurkat T cells stimulated with 1 µM TG and TG combined with anti-CD3 antibody-coated beads (1 mM and 20 mM $[Ca^{2+}]_o$ double pulse protocol as in **Fig. 6A**). Average clearance rates of single iso-cells (left column) and their ratios (right column) were determined during the first 10 s after removal of external Ca^{2+}. Error bars indicate S.E.M., numbers within the bars indicate the number of iso-cells. Iso-cells had plateau ratios between 0.95 and 1.05. Arrest in G_2/M phase was analyzed as well; the data is not shown because SOCE was inhibited during mitosis as previously reported and only very small clearance rates could be determined.

Movie 1 Full time-lapse recording of the Jurkat-Raji contact depicted in Supplementary Figure 1**A**. ORAI1-mEGFP (green), Lifeact-mRFPruby (red), anti-CD3 Alexa647 (magenta) and Fura-2 (blue) channels are merged and displayed as 3-dimensional maximum intensity projection (MIP). Scale bar is 5 µm, dotted lines indicate the coverslip position. Time interval is 1 min.

Movie 2 Full time-lapse recording of the Jurkat-Raji contact depicted in Figure 1**A**. ORAI1-mEGFP (green), STIM1-TagRFP-T (red) and Fura-2 (blue) channels are merged and displayed as 3-dimensional maximum intensity projections (MIP). Scale bar is 5 µm, dotted lines indicate the coverslip position. Time interval is 2 min.

Movie 3 Full time-lapse recording of the Jurkat-Raji contact depicted in Supplementary Figure 1**A** (only ORAI1-mEGFP). ORAI1-mEGFP channel is displayed as 3-dimensional maximum intensity projection (MIP). Scale bar is 5 µm, dotted lines indicate the coverslip position. Time interval is 1 min.

Movie 4 Time-lapse recording of a Lifeact-mRFPruby (red) expressing Jurkat T-cell making contact with an anti-CD3 antibody-coated bead. Brightfield pictures are weakly merged to visualize the beads. Images were acquired with Nyquist sampling. Scale bar is 5 µm, dotted lines indicate the coverslip position and time interval is 1 min. The video was compressed using the codec "Microsoft Windows Media Video 9".

Movie 5 Full time-lapse recording of the Jurkat-Raji contact depicted in Figure 1**C**. EGFP-PMCA4b (green) and Fura-2 (blue) channels are merged and displayed as 3-dimensional maximum intensity projections (MIP). Scale bar is 5 µm, dotted lines indicate the coverslip position. Time interval is 2 min.

Mathematical model for the effect of mitochondria relocation on global Ca^{2+} concentration

I. MODEL DEFINITION

The model that we describe in the main text (and that is sketched in Fig. 9A) is mathematically formulated as a one-dimensional diffusion equation with source, sinks and appropriate boundary conditions:

$$\frac{\partial c(x,t)}{\partial t} = D\frac{\partial^2 c(x,t)}{\partial x^2} - k_{\mathrm{PMCA_{IS}}}\, c(x_0,t)\,\delta(x-x_0) - k_{\mathrm{in}}\, c(x_{\mathrm{in}},t)\,\delta(x-x_{\mathrm{in}}) + k_{\mathrm{in}}\, c(x_{\mathrm{in}},t)\,\delta(x-x_{\mathrm{out}})\ . \tag{1}$$

with boundary condition

$$Dc_s'(x=0) = \left.\frac{dc_s}{dx}\right|_{x=0} = -k_{\mathrm{CRAC}} \qquad \text{and} \qquad Dc_s'(x=L) = \left.\frac{dc_s}{dx}\right|_{x=L} = +k_{\mathrm{PMCA}} c_s(x=L)\ . \tag{2}$$

The variable x denotes the distance from the IS, x_0 is the distance of the IS-PMCAs from the IS, x_{in} and x_{out} the distance of the mitochondria entry and release points from the IS, and L the size of the (one-dimensional) cell and simultaneously the distance of additional PMCAs form the IS. k_{CRAC}, k_{PMCA} and $k_{\mathrm{PMCA_{IS}}}$ are the strengths of the CRAC channel and PMCA pumps at the IS and the rear end of the cell, respectively, and , k_{in} the strength of the mitochondrial uptake (determining also the release at the other end of the mitochondria $k_{\mathrm{out}} = k_{\mathrm{in}} c_s(x = x_{\mathrm{in}})$.

II. MODEL SOLUTION

We are interested in the stationary solution $c_s(x) = \lim_{t\to\infty} c(x,t)$, that is reached quickly due to fast Ca^{2+}-diffusion. For this holds $c_s''(x) = 0$ for $x \neq x_{\mathrm{in}}, x_{\mathrm{out}}$, implying that the function $c_s(x)$ is piecewise linear (as depicted in Fig. 1) and of course continuous. At the points $x = x_{\mathrm{in}}$ and $x = x_{\mathrm{out}}$ the 2nd derivative of $c_s(x)$ has a delta-function part

$$Dc_s''(x) = +k_{\mathrm{in}} c_s(x_{\mathrm{in}})\delta(x-x_{\mathrm{in}}) - k_{\mathrm{PMCA_{IS}}}\, c(x_0,t)\,\delta(x-x_0) - k_{\mathrm{in}} c_s(x_{\mathrm{in}})\delta(x-x_{\mathrm{out}})\ , \tag{3}$$

i.e. the 1st derivative jumps by

$$\Delta c_s'(x_{0,\text{in,out}}) = \lim_{\epsilon\to 0}\int_{x_{0,\text{in,out}}-\epsilon}^{x_{0,\text{in,out}}+\epsilon} dx\; c_s''(x) \;=\; \begin{cases} c_s(x_0)\,k_{\text{PMCA}_{\text{IS}}} & \text{for} \quad x = x_0 \\ c_s(x_{\text{in}})\,k_{\text{in}} & \text{for} \quad x = x_{\text{in}} \\ -c_s(x_{\text{in}})\,k_{\text{in}} & \text{for} \quad x = x_{\text{out}} \end{cases} \tag{4}$$

As in Fig. 1 we denote $c_{\text{IS}} = c_s(x = x_{\text{IS}})$, $c_0 = c_s(x = 0)$, $c_1 = c_s(x = x_{\text{in}})$, $c_2 = c_s(x = x_{\text{out}})$ and $c_3 = c_s(x = L)$. Moreover we define $l = x_{\text{out}} - x_{\text{in}}$, the length of the mitochondria, and the slopes $\Delta_{\text{IS}} = (c_{\text{IS}} - c_0)/x_0$, $\Delta_0 = (c_0 - c_1)/(x_{\text{in}} - x_0)$, $\Delta_1 = (c_2 - c_1)/l$ and $\Delta_2 = (c_2 - c_3)/(L - x_{\text{out}})$, implying

$$\begin{aligned} c_0 &= c_{\text{IS}} - \Delta_{\text{IS}} x_0 \\ c_1 &= c_0 - \Delta_0(x_{\text{in}} - x_0) \\ c_2 &= c_1 + \Delta_1 l \\ c_3 &= c_2 - \Delta_2(L - x_{\text{out}}) \end{aligned} \tag{5}$$

In addition we have from the boundary conditions (2)

$$\begin{aligned} \Delta_{\text{IS}} &= k_{\text{CRAC}}/D \\ \Delta_2 &= c_3 k_{\text{PMCA}}/D \end{aligned} \tag{6}$$

and from the jump conditions (4)

$$\begin{aligned} D\Delta_{\text{IS}} - D\Delta_0 &= c_0 k_{\text{PMCA}_{\text{IS}}} \\ D\Delta_0 + D\Delta_1 &= c_1 k_{\text{in}} \\ D\Delta_1 + D\Delta_2 &= c_1 k_{\text{in}}\ , \end{aligned} \tag{7}$$

which immediately gives $\Delta_2 = \Delta_0$ as already indicated in Fig. 9A. A bit of algebra leads to the solution

$$\begin{aligned} \Delta_0 = \Delta_2 &= \frac{k_{\text{CRAC}}}{k_{\text{PMCA}_{\text{IS}}}} \frac{1}{a_0 - a_1 b_0/b_1} \\ \Delta_1 &= -\Delta_0 \frac{b_0}{b_1} \\ c_3 &= \tfrac{D}{k_{\text{in}}}(\Delta_0 + \Delta_1) + \Delta_1 l - \Delta_0(L - x_{\text{out}}) \\ c_2 &= \tfrac{D}{k_{\text{in}}}(\Delta_0 + \Delta_1) + \Delta_1 l \\ c_1 &= \tfrac{D}{k_{\text{in}}}(\Delta_0 + \Delta_1) \\ c_0 &= \tfrac{k_{\text{CRAC}}}{k_{\text{PMCA}_{\text{IS}}}} - \Delta_0 \tfrac{D}{k_{\text{PMCA}_{\text{IS}}}} \\ \Delta_{\text{IS}} &= \tfrac{k_{\text{CRAC}}}{D} \\ c_{\text{IS}} &= c_0 + \tfrac{k_{\text{CRAC}}}{D}\, x_{\text{in}} \end{aligned} \tag{8}$$

where

$$\begin{aligned} a_0 &= x_{\text{in}} - x_0 + \tfrac{D}{k_{\text{in}}} + \tfrac{D}{k_{\text{PMCA}_{\text{IS}}}} \\ a_1 &= \tfrac{D}{k_{\text{in}}} \\ b_0 &= -(L - x_{\text{out}}) + \tfrac{D}{k_{\text{in}}} - \tfrac{D}{k_{\text{PMCA}_{\text{IS}}}} \\ b_1 &= \tfrac{D}{k_{\text{in}}} + l \end{aligned} \tag{9}$$

In the following we will discuss this solution.

III. PARAMETER CHOICE

To be quantitative one needs estimates for the parameters. First one has to consider that that the model is one-dimensional, which means that physiologically relevant concentrations and reaction rates have to be adopted: Concentrations in one dimension are measured in number of Ca^{2+}-ions per micron, which is the inverse mean distance between Ca^{2+}-ions. In three space dimensions Ca^{2+} cc are measure in nM, i.e. in number of Ca^{2+} ions per volume. The third root of this 3d concentration yields the inverse mean distance of Ca^{2+} ions in 3d, too. For instance a Ca^{2+} cc of 100nM means 60 Ca^{2+}-ions per cubic-micron, corresponding to an average distance of 1/4 micron between Ca^{2+} ions. Thus $100nM$ corresponds in our model to a cc to $4\mu m^{-1}$ (note that increasing the cc in one dimension increases the cc in 3 dimensions by a factor 8). Thus we can translate Ca^{2+} cc in 1d (c_{1d}) to Ca^{2+} cc in 3d (c_{3d}) via the formula

$$c_{3d}\ [nM] = 1.66 \cdot (c_{1d} \cdot \mu m)^3 \tag{10}$$

Moreover inverse Ca^{2+} cc, as used for a measure of Ca^{2+} pumps, are related via $c_{3d}^{-1}\ [nM^{-1}] = 0.6 \cdot (c_{1d}^{-1} \cdot \mu m^{-1})^3$. A completely open single CRAC channel releases 1 Ca^{2+} ion per 32 μsec., which means in 3 dimensions the CRAC rate is $k_{\text{CRAC,3d}} = 3 \cdot 10^5 \text{sec}^{-1}$. In one dimension this corresponds to $k_{\text{CRAC}} = 100\ \text{sec}^{-1}$.

In the absence of PMCAs at the IS one can show (see below) that $c_3 = k_{\text{CRAC}}/k_{\text{PMCA}}$. When we assume that at $x = L$ (the point with the largest distance from the IS) the Ca^{2+} cc is "normal", then $c_3 = c_{\text{rest}} = 4\mu m^{-1}$. Since also k_{CRAC} is fixed we have for the PMCA rate $k_{\text{PMCA}} = 25\mu\ \text{sec}^{-1}$. When PMCAs are present at the IS we assume that their combined capacity is stronger than that of the PMCAs at the opposite end. In the following we consider the Mito rate k_{in} in relation to k_{PMCA}. The Ca^{2+} diffusion constant is set to $D = 100\mu m^2 \text{sec}^{-1}$, the cell size is $L = 100\mu m$ and the mito length is $l = 1\mu m$. The

	1d model	3d equivalent
$c_{\rm rest}$	4 μm^{-1}	0.1 μM
$k_{\rm CRAC}$	200 sec^{-1}	$3{\cdot}10^5$ sec^{-1}
$k_{\rm PMCA}$, $k_{\rm PMCA_{IS}}$	20 μm sec^{-1}	$4.8{\cdot}10^6$ μM^{-1}sec^{-1}
$k_{\rm in}$	50 μm sec^{-1}	$75{\cdot}10^6$ μM^{-1}sec^{-1}
D	100 μm^2sec^{-1}	
L	10 μm	
$l = x_{\rm out} - x_{\rm in}$	1 μm	
x_0	0.1 μm	
$x_{\rm in}$	0.2 – 5 μm	

parameters are summarized in table 1.

IV. RESULTS

The effect of changing the position $x_{\rm in}$ of the mitochondria is most easily seen when neglecting the PMCAs at the IS. Then $x_0 = 0$ and $c_{\rm IS} = c_0$ and the solution of the remaining quantities is

$$\begin{aligned} c_3 &= k_{\rm CRAC}/k_{\rm PMCA} \\ c_2 &= k_{\rm CRAC}/k_{\rm PMCA} + k_{\rm CRAC}(L - l - x_{\rm in})/D \\ c_1 &= \frac{k_{\rm CRAC}/k_{\rm PMCA} + k(L - x_{\rm in})}{1 + k_{\rm in} l/D} \\ c_0 &= \frac{k_{\rm CRAC}/D}{1 + k_{\rm in} l/D}(L + D/k_{\rm PMCA} + x_{\rm in} k_{\rm in} l/D) \end{aligned} \tag{11}$$

From eq.(11) one observes immediately that independent of the choice of parameter values the Ca^{2+} cc at the IS, c_0, increases with increasing distance between the mitos and the CRAC channels (i.e increasing $x_{\rm in}$) and that the Ca^{2+} cc in the center of the cell (i.e the average $(c_2{+}c_3)/2$) decreases with increasing $x_{\rm in}$. Thus the model predicts that mitochondria relocation towards the IS is sufficient to increase the global Ca^{2+} concentration when CRAC channels are active. Concomitantly the Ca^{2+} cc at the IS is reduced when mitos are close to the IS.

This remains true for the model *with* the PMCAs at the IS, for which we evaluate the solution (8) numerically. Using the parameter defined above we have calculated $c_s(x)$ using

eq.(8). In Fig. 9B of the main text we show the Ca^{2+} concentration as a function of x for different positions $x_{\rm in}$ of the mitochondria and different mito rates $k_{\rm in}$. As expected the Ca^{2+} cc at the IS decreases with decreasing distance of the mitos, whereas the Ca^{2+} cc in the bulk increase with decreasing distance. The effect is most pronounced for high mito rates, where also the Ca^{2+} cc at the IS is, as expected, lowest.

In Fig. 9C of the main text we compare the average Ca^{2+} cc in the IS micro-domain,

$$\overline{c}_{\rm IS} = (c_{\rm IS} + c_0)/2 \tag{12}$$

with the average global Ca^{2+} cc, c_{global} defined as

$$\begin{aligned} \overline{c}_{\rm global} &= L^{-1} \int_0^L dx\, c_s(x) \\ &= x_0(c_{\rm IS} + c_0)/2 \,+\, (x_{\rm in} - x_0)(c_0 + c_1)/2 \,+\, l(c_1 + c_2)/2 \,+\, (L - x_{\rm out})(c_2 + c_3)/2\,. \end{aligned} \tag{13}$$

In addition to the general trend that the global and IS Ca^{2+} cc follow opposite trends when varying the distance $x_{\rm in}$ one sees that for large mito rates the global Ca^{2+} cc can even be higher than the Ca^{2+} cc at the IS when the mitochondria are close to the IS. Here the increase of the global Ca^{2+} cc when moving mitos from the center of the cell to the IS is about 50%.

One might expect that moving a strong sink closer to the main Ca^{2+} source will decrease the Ca^{2+} cc here and that the release of this absorbed Ca^{2+} at a distant site will increase the Ca^{2+} cc there. But that the *total* amount of Ca^{2+} present in the cell will be substantially *increased* already by this simple redistribution without any further mechanisms involved appears to be a rather non-trivial prediction of this simple model.